Journal of Molecular Liquids 312 (2020) 113381

Contents lists available at ScienceDirect

Journal of Molecular Liquids

journal homepage: www.elsevier.com/locate/molliq

Soret effect in lyotropic liquid crystal in the isotropic phase revealed by time-resolved thermal lens

G.M. Oliveira [a], V.S. Zanuto [a], G.A.S. Flizikowski [a], N.M. Kimura [a], A.R. Sampaio [a], A. Novatski [b], M.L. Baesso [a], L.C. Malacarne [a], N.G.C. Astrath [a,*]

[a] Department of Physics, Universidade Estadual de Maringá, Maringá, PR 87020-900, Brazil
[b] Department of Physics, Universidade Estadual de Ponta Grossa, Ponta Grossa, PR 84010-330, Brazil

ARTICLE INFO

Article history:
Received 6 April 2020
Received in revised form 13 May 2020
Accepted 15 May 2020
Available online 18 May 2020

Keywords:
Soret effect
Thermodiffusion
Thermal Lens
Lyotropic liquid crystal
Mass diffusion

ABSTRACT

We demonstrate the Soret effect in a lyotropic liquid crystal at different temperatures across the isotropic phase detected by the time-resolved thermal lens technique. We investigate thermo-optical and mass diffusion properties of the sample and present quantitative characterization of Soret, mass and thermal diffusion coefficients. The results reveal that the temperature gradient induced in the experiments causes the migration of micelles from hotter to colder regions in the sample. The increase of the mass diffusion coefficient with temperature is related to the decrease of the radius of the micelles in the solution.

1. Introduction

Lyotropic liquid crystals are formed by dissolving amphiphilic molecules in a solvent (usually water). The self-assembly of amphiphilic molecules in excess water are influenced by the structural characteristics of the amphiphilic molecule and the conditions of the solution. As the surfactant concentration in the solution (c) exceeds the critical micellar concentration (CMC), different polymorphic structures can be observed. At low concentrations of amphiphilic ($c \approx$ CMC) spherical micelles are formed with typical diameter of about twice the length of the surfactant carbon chain, which results in a clear and isotropic solution. At amphiphilic concentrations greater than 100 CMC, although randomly oriented in space in an isotropic phase, micelles with non-spherical shape can be observed [1]. Micellar isotropic phase is optically isotropic, with a single index of refraction. The characteristic X-ray diffraction pattern of this phase presents a small-angle scattering due to the individual micelles, with a modulus of the scattering vector $s \approx 2 \times 10^{-2}$ nm^{-1} [2].

The order of stability of different lyotropic phases varies as a function of concentration (and of temperature) of amphiphilic molecules in water. At high concentrations, micelles aggregate forming ordered structures leading to hexagonal, cubic or lamellar phases, for instance [3]. Furthermore, at high concentrations, nematic and cholesteric phases are also obtained [4–7]. The lyotropic isotropic phase is useful for numerous potential applications, especially for encapsulation of a wide range of target molecules or controlled release drugs [8–13]. The particular properties of each structural phase lead to different diffusion coefficients in the solution, which depend on temperature and on the micellar concentration.

Mass diffusion may be induced within a fluid mixture by a temperature gradient. The spatial temperature distribution is the driving force that causes migration of components in the mixture from regions with different temperatures. This effect is known as thermodiffusion or the Soret effect. The Soret coefficient (S_T) determines the magnitude of thermodiffusion in the steady state. Thermodiffusion is observed in a variety of molecular systems, including gases, simple and multicomponent liquid mixtures [14]. The Soret effect is relevant in many fields including applications in the manipulation of macromolecules in biology [14–16], separation processes in polymer solutions [17,18], and colloidal dispersions [19–21]. The drift of dispersed particles due to a thermal gradient allows contact-free molecular segregation [22,23] and has been used to manipulate molecules for DNA trapping [24–26]. Detection of thermal diffusion in liquid mixtures is feasible with many different experimental approaches [27,28]. Thermodiffusion can be detected by pump-probe methods, such as the thermal lens method [20,29,30], grating methods [31–33], thermal diffusion cells [34–36], thermogravitational columns [37], field-flow fractionation [38], and microscopic methods [39,40].

* Corresponding author.
E-mail address: ngcastrath@uem.br (N.G.C. Astrath).

https://doi.org/10.1016/j.molliq.2020.113381
0167-7322/

The time-resolved thermal lens method has been very successful in accessing thermal, optical and mass diffusion properties of a variety of solutions [41–46]. In the usual configuration of the thermal lens method, a continuous Gaussian laser beam is used to induce a thermal gradient in the sample, which initially follows the same profile of the radial intensity distribution of the excitation beam. This localized thermal perturbation changes the refractive index accordingly causing an optical path variation in the excited volume of the sample probed by a second continuous laser beam, which has its wavefront distorted. The transient signal is monitored at the far-field detector by measuring the probe beam on-axis intensity variation. Additionally, a concentration gradient produced by the drift of disperse particles due to the thermal gradient in the fluid mixture may also take place [29]. This effect causes a thermally induced concentration gradient and thus an additional phase shift to the probe beam. The thermal lens measures a convoluted signal arising from the wavefront distortions caused by both the thermal and concentration gradients in the sample, simultaneously.

In this work, we present a quantitative analysis of thermo-optical and mass diffusion properties of a lyotropic liquid crystal in the isotropic phase at different temperatures using the thermal lens method. The sample is a mixture of potassium laurate, decanol and water. Mass diffusion coefficient and the thermal diffusivity of the sample were obtained directly from the thermal lens transients. Additional measurements of the temperature and concentration coefficients of the refractive index were performed. The results were used to determine the Soret coefficient and to estimate the radius of the micelles in the solution.

2. Theory

In a typical thermal lens experimental setup, the sample is excited by a continuous TEM_{00} laser beam for a duration of $0 < t \le \xi$ (laser-on). The excitation is turned off for $t > \xi$ (laser-off). Detecting laser-off transients is important to distinguish Soret effect from other photoinduced effects, such as photoinduced chemical reaction [44,47]. Considering an isotropic and weakly absorbing material, the temperature rise distribution in a sample is described by the heat conduction differential equation [44]

$$\frac{\partial T(r,z,t)}{\partial t} - D_{\mathrm{th}}\nabla^2 T(r,z,t) = Q_0 e^{-2r^2/w^2}[1-\mathrm{H}(t-\xi)], \tag{1}$$

where $D_{\mathrm{th}} = k/\rho c$ is the thermal diffusivity, k is thermal conductivity, ρ is mass density and c is the specific heat of the sample. $Q_0 = 2PA/\rho c\pi w^2$, w and P are the radius and power of the excitation laser, respectively, and A is the optical absorption coefficient at the excitation wavelength λ_e. The Heaviside Theta function, $\mathrm{H}(x)$, accounts for the laser-on/off excitation. The heat produced by the absorption of the excitation beam is treated as a line heat source, and the sample as an infinite medium with respect to the excitation beam radius. The heat conduction equation is solved using integral transform methods (Laplace, Fourier cosine, and Hankel transform methods), yielding

$$T(r,t) = Q_0 \int_{t_0}^{t} \frac{\exp\left(-\dfrac{2r^2/w^2}{1+2\tau/t_c}\right)}{1+2\tau/t_c} \mathrm{d}\tau, \tag{2}$$

with $t_0 = 0$ for $t \le \xi$ and $t_0 = t - \xi$ for $t > \xi$. Eq. (2) describes the temperature profile in the sample during laser-on and laser-off periods. The characteristic heat diffusion time constant is $t_c = w^2/4D_{\mathrm{th}}$.

The thermal gradient may also induce a concentration gradient – the Soret effect, which is given by the mass flow diffusion equation for a binary mixture in the absence of convection [44].

$$\frac{\partial c(r,t)}{\partial t} - D_{\mathrm{m}}\nabla^2 c(r,t) = S_{\mathrm{T}}\bar{c}(1-\bar{c})D_{\mathrm{m}}\nabla^2 T(r,t), \tag{3}$$

where D_{m} is the mass diffusion coefficient, $\bar{c}$ is the initial average concentration and $S_{\mathrm{T}} = D_{\mathrm{T}}/D_{\mathrm{m}}$ is the Soret coefficient. D_{T} denotes the coefficient of thermal diffusion and the characteristic mass diffusion time is defined as $t_{\mathrm{m}} = w^2/4D_{\mathrm{m}}$. Usually $t_{\mathrm{m}} \gg t_c$, and then for $t \gg t_c$, $\nabla^2 T(r,t)$ in Eq. (3) can be replaced by the stationary solution of the heat conduction equation; right hand side of Eq. (1) [20,44]. Using this approximation, the mass diffusion equation presents essentially the same form as that of the heat conduction equation. The sample is sufficiently thick so that the axial null thermal flux approximation can be applied and the viscous surface effects can be neglected. Assuming that the volume excited by the laser beam is much smaller than the sample dimensions, the solution of the mass flow diffusion equation is

$$c(r,t) = -S_{\mathrm{T}}\bar{c}(1-\bar{c})\frac{D_{\mathrm{m}}}{D_{\mathrm{th}}}Q_0 \int_{t_0}^{t} \frac{\exp\left(-\dfrac{2r^2/w^2}{1+2\tau/t_{\mathrm{m}}}\right)}{1+2\tau/t_{\mathrm{m}}} \mathrm{d}\tau. \tag{4}$$

When a TEM_{00} Gaussian probe laser beam propagates through the excited volume of the liquid sample, its wavefront is slightly distorted, and the distortion can be expressed as an additional phase shift. This phase shift can be calculated by considering the problem from the point of view of optical path length variation along the propagation axis as $\phi(r,t) = (2\pi/\lambda_{\mathrm{p}})\int_0^L [n(r,z,t) - n(0,z,t)]\mathrm{d}z$. $n(r,z,t)$ is the time dependent spatial distribution of the refractive index, L is the sample thickness, and λ_{p} is the probe beam wavelength. The total additional phase shift when both the thermal and the Soret effects occur is the superposition of the phase shifts, ϕ_{th} and ϕ_{Soret}, caused by the temperature mass gradient (Soret effect) [44], respectively. Both effects give rise to two z-independent refractive index gradients that act as an optical element in the sample. The phase shifts are given by

$$\phi_{\mathrm{th}}(r,t) = \frac{2\pi}{\lambda_{\mathrm{p}}} L \frac{dn}{dT}[T(r,t) - T(0,t)], \tag{5}$$

and

$$\phi_{\mathrm{Soret}}(r,t) = \frac{2\pi}{\lambda_{\mathrm{p}}} L \frac{dn}{dc}[c(r,t) - c(0,t)]. \tag{6}$$

The temperature and concentration coefficients of the refractive index at the probe beam wavelength are dn/dT and dn/dc, respectively. In other words, the phase shift describes the distortions of the probe beam caused by the temperature and concentration changes in the medium. From Eq. (5) using Eq. (2), ϕ_{th} can be calculated as

$$\phi_{\mathrm{th}}(g,t) = \frac{\theta_{\mathrm{th}}}{t_c} \int_{t_0}^{t} \frac{1 - \exp\left(-\dfrac{2mg}{1+2\tau/t_c}\right)}{1+2\tau/t_c} \mathrm{d}\tau. \tag{7}$$

From Eq. (6), using Eq. (4), the phase shift produced by the Soret effect is

$$\phi_{\mathrm{Soret}}(g,t) = \frac{\theta_{\mathrm{m}}}{t_{\mathrm{m}}} \int_{t_0}^{t} \frac{1 - \exp\left(-\dfrac{2mg}{1+2\tau/t_{\mathrm{m}}}\right)}{1+2\tau/t_{\mathrm{m}}} \mathrm{d}\tau. \tag{8}$$

In Eqs. (7) and (8), the variables $g = (r/w_{\mathrm{p}})^2$ and $m = (w_{\mathrm{p}}/w)^2$ have been introduced, where w_{p} is the radius of the probe laser beam in the sample. In addition, θ_{th} and θ_{Soret} are defined respectively as

$$\theta_{\mathrm{th}} = -\frac{PAL}{k\lambda_{\mathrm{p}}}\frac{dn}{dT}, \tag{9}$$

and

$$\theta_{\mathrm{Soret}} = S_{\mathrm{T}}\bar{c}(1-\bar{c})\frac{PAL}{k\lambda_{\mathrm{p}}}\frac{dn}{dc}. \tag{10}$$

The total phase shift is

$$\phi_{TL}(g,t) = \phi_{th}(g,t) + \phi_{Soret}(g,t). \quad (11)$$

The propagation of the emergent probe beam from the sample to the detector plane can be treated as a diffraction phenomenon, and calculated using Fresnel diffraction theory [48]. The intensity at the center of the probe beam spot at the detector plane is given by

$$I(t) = \left| \int_0^\infty \exp\left[-\left(1 + i\frac{z_1}{z_c}\right)g - i\phi_{TL}(g,t) \right] dg \right|^2, \quad (12)$$

where z_c is the confocal distance of the probe beam and z_1 is the distance from the probe beam waist to the sample. Eq. (12) can be evaluated numerically using the calculated ϕ_{th} and ϕ_{Soret}.

3. Material and methods

The thermal lens method was used to evaluate the thermo-optical and mass transport properties of a lyotropic liquid crystal in the isotropic phase. The sample is a mixture of potassium laurate (KL), decanol (DeOH, Sigma-Aldrich, p.a. >99%) and deionized/distilled water with the concentration of 26.89 wt% of KL, 6.39 wt% of DeOH and 66.72 wt% of H_2O. For this mixture the relative molar concentration, $C = [KL]/[DeOH]$, is 2.79. Potassium laurate was synthesized from lauric acid via neutralization with potassium hydroxide and was further purified by being recrystallized with ethanol several times. The sample was prepared following the same procedure used in Ref. [49]. This lyotropic phase was characterized as a function of the temperature by means of optical microscopy and presented the isotropic phase in the range of 10°C to 45°C.

Fig. 1 shows the time-resolved thermal lens experimental apparatus used in this work. A continuous DPSS Nd:YAG laser (TEM_{00}, wavelength $\lambda_e = 532$ nm) was used as the excitation beam. A shutter controlled the exposure of the sample to the excitation beam, and the signal from the photodiode (PD Trigger) triggered the digital oscilloscope that recorded the thermal lens signal. The sample was horizontally placed in a 5-mm optical path quartz cuvette and the excitation beam was perpendicular to its surface. This arrangement minimizes the effects of gravity on the mass transport within the sample [20]. A continuous He—Ne laser (TEM_{00}, wavelength $\lambda_p = 632.8$ nm), of significantly weaker intensity, was used as a probe beam. Both beams were focused by biconvex lenses L_i with focal distances f_i. The angle between the excitation and probe beams is <1°. After passing through the sample, the probe beam was propagated to the far field (~5 m) where its on-axis intensity variation was detected by a photodiode (PD TL) connected to an oscilloscope. A pinhole-filter (at 632.8 nm) assembly was placed in front of the photodiode to detect only the central part of the probe beam intensity variation. A heating unit and a temperature controller were used to control the sample temperature with a precision better than 0.01°C in the range between 20°C and 35°C. The laser beam radius at the sample was $w = 75$ μm for the excitation and $w_p = 375$ m for the probe, $z_1 = 24$ cm, and $z_c = 9.5$ cm. These experimental parameters were determined as described in Ref. [48].

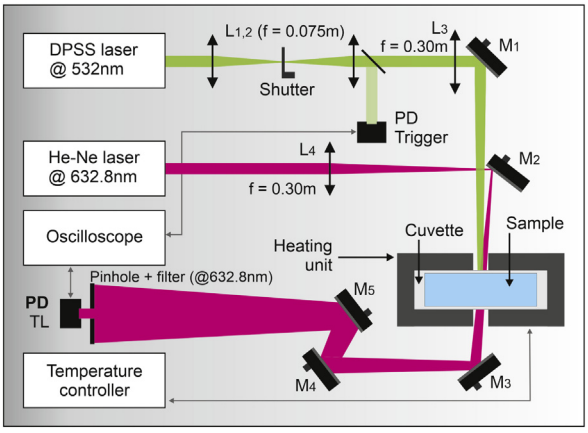

Fig. 1. Schematic diagram of the time-resolved thermal lens experimental apparatus. M_i, L_i, and PD stand for mirrors, lenses, and photodiodes, respectively.

Density analysis was performed using a digital density meter (Anton Paar, DMA 5000), from 20°C to 35°C. Refractive index measurements were performed as a function of temperature and concentration of [KL + DeOH] in water. Specific heat measurements were performed in a home-made thermal relaxation calorimeter [50]. The temperature coefficient of the refractive index (dn/dT) was measured using an optical interferometer experimental system, as described in details in Ref. [51]. In this method, the sample is heated uniformly, and the interference between the reflections of a He—Ne laser beam at 632.8 nm from both cuvette surfaces creates a temperature dependent interferogram, which can be used to calculate dn/dT.

4. Results and discussion

We have performed thermal lens temperature dependent experiments in the isotropic phase of KL-DeOH-water using four different excitation powers. The results for the normalized thermal lens signals, $I(t)/I(0)$, for the excitation powers of $P = 76$ mW and $P = 120$ mW are presented in Fig. 2. The transients (average of over 100 measurements) show the probe beam intensity variation sensed at the photodetector for the laser-on excitation regime ($t = \xi \leq 5$ s), and the laser-off ($t > 5$ s) relaxation curve.

At very short time, $t < 300$ ms, the curves resemble that of a pure thermal effect, in which a thermally induced refractive index gradient dominates the signal [41]. Subsequently, the signal follows a slow decrease of the probe beam intensity at the detector. Such a behavior is a characteristic signature of the Soret effect. This effect has been previously reported [44] and can have different contributions to the transient depending on the magnitude and signal of the Soret coefficient. For instance, a slow decrease of the probe beam intensity is due to a positive Soret coefficient. On the other hand, a negative Soret coefficient would increase the signal slowly.

The laser-off transient is also very important to distinguish the prevalent effect taking place after the laser is turned off [52]. For example,

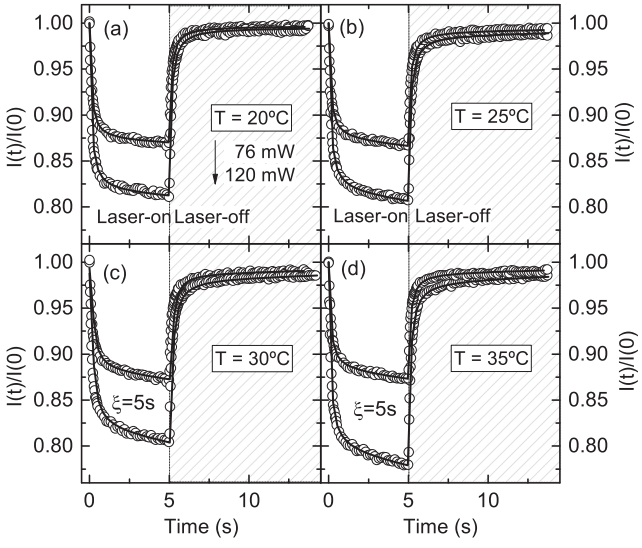

Fig. 2. Experimental thermal lens signals $I(t)/I(0)$ (open circles) at different temperatures (a)–(d) for two excitation powers. Continuous lines denote the least-square curve fits using Eq. (12).

after the laser is turned off at $t = \xi$, a pure thermal effect would appear as a rapid change in probe beam intensity approaching $I(t)/I(0) = 1$. This is not the case observed for the sample under investigation, as we can see a very slow relaxation process. The temperature gradient causes the species migration within the excited volume of the sample and establish a concentration gradient leading to the Soret effect observed.

Continuous lines in Fig. 2 display the numerical curve fits of the experimental on/off transients to $I(t)$, Eq. (12). The parameters θ_{th}, θ_{Soret}, t_c and t_m are retrieved from the fits. Thermal diffusivity D_{th} and mass diffusion coefficient D_m are calculated using the relations $D_{th} = w^2/4t_c$ and $D_m = w^2/4t_m$, respectively. The result shows an excellent agreement between the experimental and the theoretical predictions, and demonstrates that the effect of mass diffusion in the thermal lens signal are extremely well described by the proposed model, with a numerical confidence in the values are higher than 99%.

The amplitude of thermal (θ_{th}) and Soret (θ_{Soret}) effects are linearly dependent on the excitation power. The temperature dependence of the excitation power normalized amplitudes, θ_{th}/P and θ_{Soret}/P, are shown in Fig. 3 (a). Fig. 3 (b) presents the temperature dependence of thermal diffusivity and mass diffusion coefficient. The thermal diffusivities of the sample, approximately 1.1×10^{-7} m^{2}s^{-1}, are slightly below the value of 1.45×10^{-7} m^{2}s^{-1} for pure water and close to previously reported data for lyotropic mixtures in the nematic calamitic phase [41]. The mass diffusion coefficient, on the other hand, increases with the temperature reaching a value of $D_m = (4.8 \pm 0.2) \times 10^{-10}$ m^{2}s^{-1} at 35°C, in agreement with previously reported data [53].

The parameters θ_{th}/P and θ_{Soret}/P are correlated by Eqs. (9) and (10), and can provide additional information on the Soret coefficient by using the relation

$$S_T = -\frac{1}{\bar{c}(1-\bar{c})}\frac{\theta_{Soret}/P}{\theta_{th}/P}\frac{dn/dT}{dn/dc}. \quad (13)$$

The temperature coefficient of refractive index was measured using an optical interferometer. A typical interference pattern is presented in Fig. 4 (a) from which dn/dT can be obtained by identifying the maxima and minima of the intensity variation as a function of the temperature, as described in details in Ref. [51]. The measured value of $dn/dT = -(1.76 \pm 0.02) \times 10^{-4}$ K^{-1} was approximately constant over the temperature range from 20°C to 35°C. To measure the concentration coefficient of the refractive index, samples with different concentrations of [KL + DeOH] relative to water were prepared. Fig. 4 (b) shows the concentration dependence of the refractive index for different

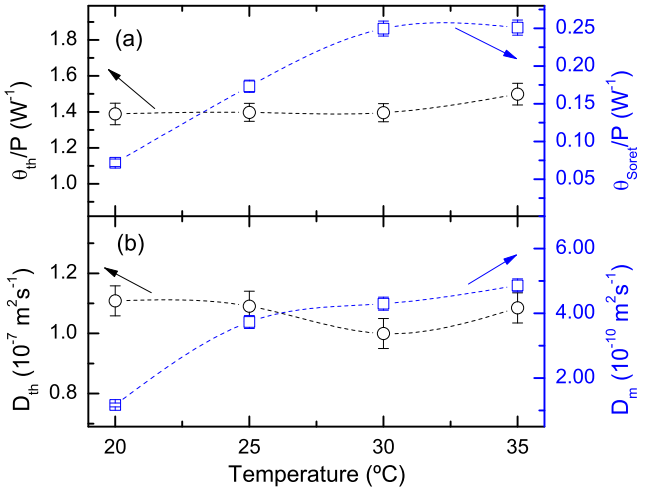

Fig. 3. Temperature dependence of (a) the excitation power normalized amplitudes of thermal and Soret effects, θ_{th}/P and θ_{Soret}/P, respectively, and of (b) the thermal diffusivity and the mass diffusion coefficient of the sample. Dashed lines are guides to the eye.

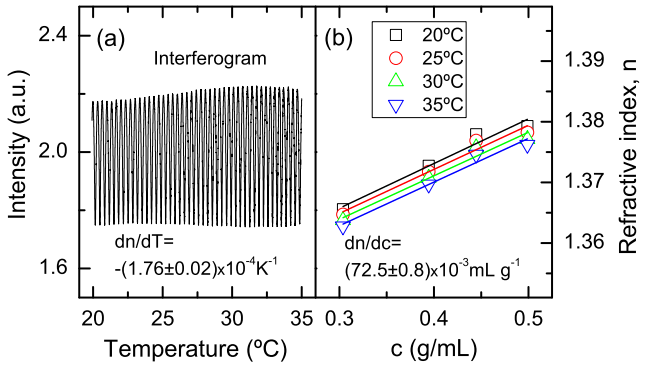

Fig. 4. (a) Temperature dependence of the interference pattern. (b) Refractive index dependence on the concentration of [KL + DeOH] in water. Continuous lines represent linear regressions.

temperatures. Continuous lines represent linear regressions and the value of $dn/dc = (72.5 \pm 0.8) \times 10^{-3}$ mLg^{-1} was found to be constant in this temperature range.

The thermal conductivity was calculated using the relation $k = \rho c D_{th}$. The mass density was measured as a function of the temperature and varied linearly from 1007 kgm^{-3} at 20°C to 999 kgm^{-3} at 35°C. The specific heat was approximately constant with the temperature, $c = (4.32 \pm 0.06)$ Jg^{-1}K^{-1}. The temperature dependence of the thermal conductivity of the sample was found to follow the same behavior as that of the thermal diffusivity. At 20°C, $k = (0.48 \pm 0.02)$ Wm^{-1}K^{-1}, which is in agreement with previously reported data [54].

Using the measured values of θ_{th}/P, θ_{Soret}/P, dn/dT and dn/dc, the Soret coefficient was calculated and the results are presented in Fig. 5. S_T increases with the temperature and present positive values. A positive coefficient indicates that the flow of micelles happens from the hotter to the colder regions within the excited volume of the sample following the laser-induced temperature gradient. The temperature dependence of $S_T(T)$ has been shown to be very well described by the empirical equation [55].

$$S_T(T) = S_T^{\infty}\left[1 - \exp\left(\frac{T^* - T}{T_0}\right)\right]. \quad (14)$$

S_T^{∞} can be thought as the high temperature thermophobic limit, T^* is the temperature at which S_T switches sign, and T_0 is the rate of exponential growth accounting for the strength of the temperatures effects. The continuous line in Fig. 5 shows the fit to Eq. (14), yielding $S_T^{\infty} = (1.8 \pm 0.3) \times 10^{-3}$ K^{-1}, $T^* = (291 \pm 1)$ K and $T_0 = (5 \pm 1)$ K. These values are within the range of previous reported data for similar materials [55]. The coefficient of thermal diffusion can also be calculated using

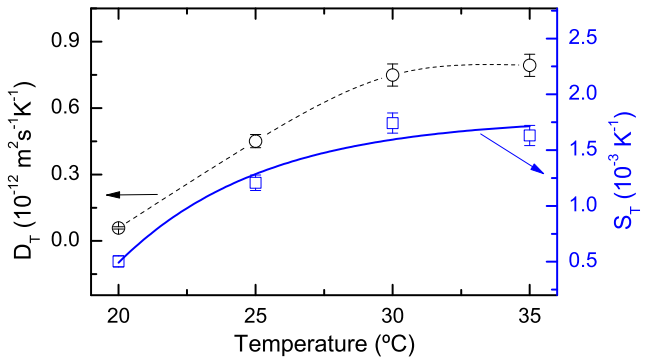

Fig. 5. Temperature dependence of the thermal diffusion coefficient and the Soret coefficient of the sample. Continuous line shows the fit of $S_T(T)$ to Eq. (14). Dashed line is a guide to the eye.

$D_T = S_T D_m$ and the results are presented in Fig. 5. The values found for this coefficient are within the expected for this solution [27].

The migration of micelles from hotter to colder regions can also be observed by looking to the relaxation processes; laser-off transient. This can be better visualized if the contributions from each effect are showed separately. Fig. 6 shows the same transient as that of Fig. 2 (d) for 35°C and excitation power of 120 mW. Continuous line (black) is the fit using both thermal (ϕ_{th}, Eq. (7)) and Soret (ϕ_{Soret}, Eq. (8)) contributions to the intensity signal, as previously presented. Dashed line (red) shows the thermal contribution only (Eq. (7)), i.e., $\theta_{Soret} = 0$. Note that the thermal contribution reaches the steady state faster than the experimental data for the laser-on/off transients. Dotted line (blue) shows the Soret contribution only (Eq. (8)), i.e., $\theta_{th} = 0$. The characteristic time for the Soret effect is ~2.85 s, which is much longer than the thermal diffusion time, ~12.8 ms, clearly explaining the laser-on/off decreasing signal observed in the transient. Although the thermal effect is the main contribution to the total thermal lens signal, the Soret effect is large enough to be characterized.

The analysis of the micellar solution using the thermal lens method provides information that correlates thermal, optical and transport properties. Assuming the spherical micelle model, as a first approximation, we can further use the results presented here to estimate the radius R of the species involved in the mass diffusion by using the Stokes-Einstein equation $D_m = k_B T/(6\pi\eta R)$ [56]. k_B is the Boltzmann's constant and η is the solvent viscosity. Using the literature values of η for water [57], the radius of the micelles are estimated to decrease from (19 ± 2) Å at 20°C to approximately (6.5 ± 0.9) Å from 25°C to 35°C. These values are slightly smaller than those reported for this sample in the nematic phase [58].

It is important to mention that in the literature there are reports of flow-induced birefringence in the isotropic phase of similar lyotropic mixtures with $2.6 \le C \le 2.9$ [59]. Considering that the local temperature variation caused in the sample by the thermal lens is very small, e.g. the highest temperature variation at $r = 0$ induced by the excitation laser is less than 70 mK, the mass gradient is indeed small. Therefore, flow-induced birefringence can be safely neglected in the thermal lens experiments.

5. Conclusions

In this work, we have studied the temperature dependence of the thermal and mass diffusion properties of a lyotropic liquid crystal in the isotropic phase. A theoretical model that incorporates laser-induced thermal and Soret effects was presented and the thermal and mass diffusion equations were solved for the laser-on/off excitation regimes. The physical parameters retrieved from the thermal lens transients were used to determine the thermal and mass diffusivities of the sample, and to calculate the thermal diffusion coefficient and the Soret coefficient. Assuming a simplified spherical shape for the micelles in the solution and using the Stokes-Einstein equation, the radius of the micelles were estimated to vary from approximately 19 Å to 6.5 Å. Our results indicate that the method used for Soret measurements is a powerful tool for monitoring thermal and mass diffusion in lyotropic liquid crystal, and may be extended to explore different phases in various liquid crystals.

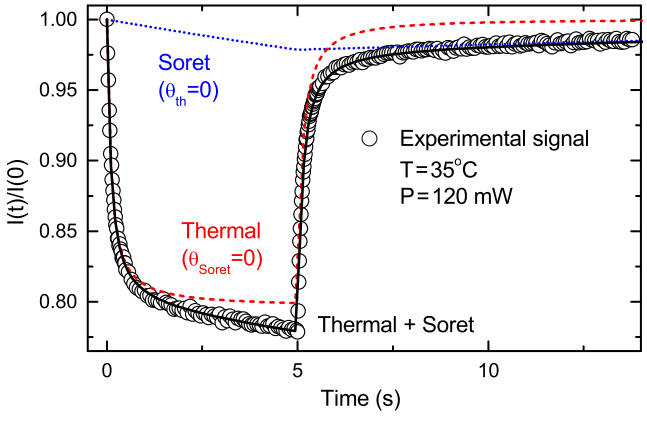

Fig. 6. Experimental thermal lens signals $I(t)/I(0)$ (open circles) at 35°C showing the contributions from: thermal and mass diffusion effects (continuous line, black); thermal effect only, $\theta_{Soret} = 0$ (dashed, red); Soret effect only, $\theta_{th} = 0$ (dotted, blue).

Acknowledgments

This work is supported by Fundação Araucária, CAPES, COPEL, INCTFCx, FAPESP and CNPq.

Funding

Coordenação de Aperfeiçoamento de Pessoal de Nível Superior - CAPES (Finance Code 001), Fundação Araucária, Companhia Paranaense de Energia - COPEL, Instituto Nacional de Ciência e Tecnologia de Fluidos Complexos - INCTFCx, Fundação de Amparo à Pesquisa do Estado de São Paulo - FAPESP (Process 2014/50983-3) and Conselho Nacional de Desenvolvimento Científico e Tecnológico - CNPq (Processes 401160/2016-5, 401460/2016-9, 465259/2014-6).

Author statement

G.M.O.: Methodology, Investigation; V.S.Z. : Investigation; G.A.S.F. : Investigation; N.M.K.: Investigation; A.R.S.: Investigation; A.N.: Investigation; M.L.B.: Investigation; L.C.M.: Investigation, Formal analysis; N.G.C.A.: Conceptualization, Writing - Review & Editing, Supervision.

Declaration of competing interest

The authors declare that they have no known competing financial interests or personal relationships that could have appeared to influence the work reported in this paper.

References

[1] S.-H. Chen, N.M. Amer, Observation of macroscopic collective behavior and new texture in magnetically doped liquid crystals, Phys. Rev. Lett. 51 (1983) 2298–2301, https://doi.org/10.1103/PhysRevLett.51.2298.
[2] A.M. Bellocq, J. Biais, P. Bothorel, B. Clin, G. Fourche, P. Lalanne, B. Lamaire, B. Lamanceau, D. Roux, Microemulsions, Adv. Colloid Interf. Sci. 20 (1984) 167–272, https://doi.org/10.1016/0001-8686(84)80005-6.
[3] S. Singh, D.A. Dunmur, Liquid Crystals: Fundamentals, World Scientific Co. Pte. Ltd, New Jersey; London; Singapore; Hong Kong, 2002https://doi.org/10.1142/4369.
[4] E. Akpinar, F. Giesselmann, M. Acimi, Interpretation of different moleular packing in the micelles of lyotropic nematic and cholesteric phases via mass density measurements, J. Mol. Liq. 200 (2014) 354–360, https://doi.org/10.1016/j.molliq.2014.11.009.
[5] E. Akpinar, S. Yurdakul, A.M. Figueiredo Neto, Comparison between lyotropic cholesteric phase behavior with partly fluorinated surfactants and their exact hydrogenated counterparts, J. Mol. Liq. 259 (2018) 239–248, https://doi.org/10.1016/j.molliq.2018.03.031.
[6] E. Akpinar, C. Canioz, M. Turkmen, D. Reis, A.M. Figueiredo Neto, Effect of the surfactant alkyl chain length on the stabilisation of lyotropic nematic phases, Liq. Cryst. 45 (2018) 219–229, https://doi.org/10.1080/02678292.2017.1309698.
[7] E. Akpinar, E. Guner, O. Demir-Ordu, A.M. Figueiredo Neto, Effect of head-group size of some tetradecylalkylammonium bromide surfactants on obtaining the lyotropic biaxial nematic phase, Eur. Phys. J. E 42 (2019) 44, https://doi.org/10.1140/epje/i2019-11806-y.
[8] T. Kaasgaard, C.J. Drummond, Ordered 2-D and 3-D nanostructured amphiphile self-assembly materials stable in excess solvent, Phys. Chem. Chem. Phys. 8 (2006) 4957–4975, https://doi.org/10.1039/B609510K.
[9] J.C. Shah, Y. Sadhale, D.M. Chilukuri, Cubic phase gels as drug delivery systems, Adv. Drug Deliv. Rev. 47 (2001) 229–250, https://doi.org/10.1016/S0169-409X(01)00108-9.
[10] L. Sagalowicz, R. Mezzenga, M.E. Leser, Investigating reversed liquid crystalline mesophases, Curr. Opin. Colloid Interface Sci. 11 (2006) 224–229, https://doi.org/10.1016/j.cocis.2006.07.002.

[11] Y. Huang, S. Gui, Factors affecting the structure of lyotropic liquid crystals and the correlation between structure and drug diffusion, RSC Adv. 8 (2018) 6978–6987, https://doi.org/10.1039/C7RA12008G.
[12] D.-H. Kim, A. Jahn, S.-J. Cho, J.S. Kim, M.-H. Ki, D.-D. Kim, Lyotropic liquid crystal systems in drug delivery: a review, J. Pharm. Investig. 45 (2015) 1–11, https://doi.org/10.1007/s40005-014-0165-9.
[13] I. Tadwee, S. Shahi, V. Ramteke, I. Syed, Liquid crystals pharmaceutical application: a review, Int. J. Pharm. Res. Allied Sci 1 (2012) 6–11.
[14] A. Parola, R. Piazza, Particle thermophoresis in liquids, Eur. Phys. J. E 15 (2004) 255–263, https://doi.org/10.1140/epje/i2004-10065-5.
[15] D. Braun, A. Libchaber, Thermal force approach to molecular evolution, Phys. Biol. 1 (2004) 1–8, https://doi.org/10.1088/1478-3967/1/1/P01.
[16] M. Eslamian, Advances in thermodiffusion and thermophoresis (soret effect) in liquid mixtures, Frontiers in Heat and Mass Transfer 2 (2011) 043001, https://doi.org/10.5098/hmt.v2.4.3001.
[17] B.-J. de Gans, R. Kita, S. Wiegand, J. Luettmer-Strathmann, Unusual thermal diffusion in polymer solutions, Phys. Rev. Lett. 91 (2003), 245501. https://doi.org/10.1103/PhysRevLett.91.245501.
[18] A. Würger, Molecular-weight dependent thermal diffusion in dilute polymer solutions, Phys. Rev. Lett. 102 (2009), 078302. https://doi.org/10.1103/PhysRevLett.102.078302.
[19] R. Piazza, A. Guarino, Soret effect in interacting micellar solutions, Phys. Rev. Lett. 88 (2002), 208302. https://doi.org/10.1103/PhysRevLett.88.208302.
[20] R. Rusconi, L. Isa, R. Piazza, Thermal-lensing measurement of particle thermophoresis in aqueous dispersions, J. Opt. Soc. Am. B. 21 (2004) 605–616, https://doi.org/10.1364/JOSAB.21.000605.
[21] S.N. Rasuli, R. Golestanian, Soret motion of a charged spherical colloid, Phys. Rev. Lett. 101 (2008), 108301. https://doi.org/10.1103/PhysRevLett.101.108301.
[22] S.A. Putnam, D.G. Cahil, G.C.L. Wong, Temperature dependence of thermodiffusion in aqueous suspensions of charged nanoparticles, Langmuir 23 (2007) 9221–9228, https://doi.org/10.1021/la700489e.
[23] R. Piazza, Thermophoresis: moving particles with thermal gradients, Soft Matter 4 (2008) 1740–1744, https://doi.org/10.1039/B805888C.
[24] D. Braun, A. Libchaber, Trapping of DNA by thermophoretic depletion and convection, Phys. Rev. Lett. 89 (2002), 188103. https://doi.org/10.1103/PhysRevLett.89.188103.
[25] S. Duhr, D. Braun, Optothermal molecule trapping by opposing fluid flow with thermophoretic drift, Phys. Rev. Lett. 97 (2006), 038103. https://doi.org/10.1103/PhysRevLett.97.038103.
[26] M. Ichikawa, H. Ichikawa, K. Yoshikawa, Y. Kimura, Extension of a DNA molecule by local heating with a laser, Phys. Rev. Lett. 99 (2007), 148104. https://doi.org/10.1103/PhysRevLett.99.148104.
[27] S. Wiegand, H. Ning, H. Kriegs, Thermal diffusion forced Rayleigh scattering setup optimized for aqueous mixtures, J. Phys. Chem. B 111 (2007) 14169–14174, https://doi.org/10.1021/jp076913y.
[28] J. Kotacz, A. Konya, R.L.B. Selinger, Q.-H. Wei, Thermophoresis of colloids in nematic liquid crystal, Soft Matter 16 (2020) 1989–1995, https://doi.org/10.1039/C9SM02424G.
[29] M. Giglio, A. Vendramini, Thermal lens effect in a binary liquid mixture: a new effect, Appl. Phys. Lett. 25 (1974) 555–557, https://doi.org/10.1063/1.1655308.
[30] N. Arnaud, J. Georges, Thermal lens spectrometry in aqueous solutions of Brij 35: investigation of micelle effects on the time-resolved and steady-state signals, Spectrochim. Acta A 57 (2001) 1085–1092, https://doi.org/10.1016/S1386-1425(00)00425-X.
[31] W. Köhler, R. Schäfer, in: M. Schmidt (Ed.), New Developments in Polymer Analytics II, 151, Springer Science, Berlin, 1999.
[32] J.C. Bacri, A. Cebers, A. Bourdon, G. Demouchy, B.M. Heegaard, R. Perzynski, Forced Rayleigh experiment in a magnetic fluid, Phys. Rev. Lett. 74 (1995) 5032–5035, https://doi.org/10.1103/PhysRevLett.74.5032.
[33] H. Ning, R. Kita, H. Kriegs, J. Luettmer-Strathmann, S. Wiegand, Thermal diffusion behavior of nonionic surfactants in water, Phys. Chem. B 110 (2006) 10746–10756, https://doi.org/10.1021/jp0572986.
[34] M. Giglio, A. Vendramini, Optical study of a convective instability in a binary liquid mixture heated from above, Optics Commun 20 (1977) 438–440, https://doi.org/10.1016/0030-4018(77)90224-3.
[35] K.J. Zhang, M.E. Briggs, R.W. Gammon, J.V.J. Sengers, Optical measurement of the Soret coefficient and the diffusion coefficient of liquid mixtures, J. Chem. Phys. 104 (1996) 6881–6892, https://doi.org/10.1063/1.471355.
[36] S.A. Putnam, D.G. Cahill, Micron-scale apparatus for measurements of thermodiffusion in liquids, Rev. Sci. Instrum. 75 (2004) 2368–2372, https://doi.org/10.1063/1.1765761.
[37] M.M. Bou-Ali, O. Ecenarro, J.A. Madariaga, C.M.J. Santamaria, Soret coefficient of some binary liquid mixtures, J. Non-Equilib. Thermodyn. 24 (1999) 228–233, https://doi.org/10.1515/JNETDY.1999.013.
[38] M.E. Schimpf, J.C. Giddings, Characterization of thermal diffusion in polymer solutions by thermal field-flow fractionation: dependence on polymer and solvent parameters, J. Polym. Sci. B: Polymer Phys. 27 (1989) 1317–1332, https://doi.org/10.1002/polb.1989.090270610.
[39] S. Rondot, O. Aaboubi, P. Baudart, D. Erre, E. Merienne, J.M. Patat, Determination of Soret coefficient and heat of transport in a binary liquid mixture using X-ray microscopy, Eur. Phys. J. AP 17 (2002) 75–80, https://doi.org/10.1051/epjap:2001005.
[40] S. Duhr, S. Arduini, D. Braun, Thermophoresis of DNA determined by microfluidic fluorescence, Eur. Phys. J. E 15 (2004) 277–286, https://doi.org/10.1140/epje/i2004-10073-5.
[41] A.C. Bento, A.J. Palangana, L.R. Evangelista, M.L. Baesso, J.R.D. Pereira, E.C. da Silva, A.M. Mansanares, Geometrical anisotropy dependence of thermal diffusivity in lyotropic nematics: mode mismatched thermal lens measurements, Appl. Phys. Lett. 68 (1996) 3371–3373, https://doi.org/10.1063/1.116507.
[42] J.R.D. Pereira, A.J. Palangana, A.M. Mansanares, E.C. da Silva, A.C. Bento, M.L. Baesso, Inversion in the change of the refractive index and memory effect near the nematic-isotropic phase transition in a lyotropic liquid crystal, Phys. Rev. E 61 (2000) 5410–5413, https://doi.org/10.1103/PhysRevE.61.5410.
[43] J.R.D. Pereira, A.M. Mansanares, A.J. Palangana, M.L. Baesso, Temperature dependence of the refractive index near the reentrant-isotropic–calamitic-nematic phase transition, Phys. Rev. E 64 (2001), 012701. https://doi.org/10.1103/PhysRevE.64.012701.
[44] L.C. Malacarne, N.G.C. Astrath, A.N. Medina, L.S. Herculano, M.L. Baesso, P.R.B. Pedreira, J. Shen, Q. Wen, K.H. Michaelian, C. Fairbridge, Soret effect and photochemical reaction in liquids with laser-induced local heating, Opt. Express 19 (2011) 4047–4058, https://doi.org/10.1364/OE.19.004047.
[45] E.L. Savi, L.C. Malacarne, M.L. Baesso, P.T.M. Pintro, C. Croge, J. Shen, N.G.C. Astrath, Investigation into photostability of soybean oils by thermal lens spectroscopy, Spectrochim. Acta Part A: Molecular and Biomolecular Spectroscopy 145 (2015) 125–129, https://doi.org/10.1016/j.saa.2015.02.106.
[46] E.L. Savi, L.S. Herculano, G.V.B. Lukasievicz, H.R. Regatieri, A.S. Torquato, L.C. Malacarne, N.G.C. Astrath, Assessing thermal and optical properties of biodiesel by thermal lens spectrometry: theoretical and experimental aspects, Fuel 217 (2018) 404–408, https://doi.org/10.1016/j.fuel.2017.12.104.
[47] N.G.C. Astrath, F.B.G. Astrath, J. Shen, J. Zhou, K.H. Michaelian, C. Fairbridge, L.C. Malacarne, P.R.B. Pedreira, A.N. Medina, M.L. Baesso, Thermal-lens study of photochemical reaction kinetics, Opt. Lett. 34 (2009) 3460–3462, https://doi.org/10.1364/OL.34.003460.
[48] J. Shen, R.D. Lowe, R.D. Snook, A model for cw laser-induced mode-mismatched dual-beam thermal lens spectrometry, Chem. Phys. 165 (1992) 385–396, https://doi.org/10.1016/0301-0104(92)87053-C.
[49] P.R.G. Fernandes, N.M. Kimura, J.N. Maki, Mechano-optical effect in isotropic phase of a lyotropic liquid crystal, Mol. Cryst. Liq. Cryst. 421 (2004) 243–252, https://doi.org/10.1080/15421400490501860.
[50] A.N. Medina, A.M.F. Caldeira, A.C. Bento, M.L. Baesso, J.A. Sampaio, T. Catunda, F.G. Gandra, Thermal relaxation method to determine the specific heat of optical glasses, J. Non-Cryst. Solids 304 (2002) 299–305, https://doi.org/10.1016/S0022-3093(02)01038-4.
[51] A. Steimacher, A.N. Medina, A.C. Bento, J.H. Rohling, M.L. Baesso, V.C.S. Reynoso, S.M. Lima, M.N. Petrovich, D.W. Hewak, The temperature coefficient of the optical path length as a function of the temperature in different optical glasses, J. Non-Cryst. Solids 348 (2004) 240–244, https://doi.org/10.1016/j.jnoncrysol.2004.08.176.
[52] L.C. Malacarne, E.L. Savi, M.L. Baesso, E.K. Lenzi, N.G.C. Astrath, Role of photophysics processes in thermal lens spectroscopy of fluids: a theoretical study, J. Phys. Chem. A 118 (2014) 5983–5988, https://doi.org/10.1021/jp505255a.
[53] P.R.G. Fernandes, A.M. Figueiredo Neto, Flow-induced birefringence in a lyotropic liquid crystal in the isotropic phase: an order diffusion approach, Phys. Rev. E 56 (1997) 6185–6188, https://doi.org/10.1103/PhysRevE.56.6185.
[54] F.L.S. Cuppo, A.M. Figueiredo Neto, Thermal and nonlinear optical properties of potassium laurate/water solutions at amphiphilic concentrations around the critical micellar concentration: a laser gaussian single beam experiment in millisecond timescales, Langmuir 18 (2002) 9647–9653, https://doi.org/10.1021/la026267o.
[55] S. Iacopini, R. Rusconi, R. Piazza, The "macromolecular tourist": universal temperature dependence of thermal diffusion in aqueous colloidal suspensions, Eur. Phys. J. E 19 (2006) 59–67, https://doi.org/10.1140/epje/e2006-00012-9.
[56] J. Georges, T. Paris, Influence of the Soret effect on the analytical signal in cw-laser thermal lens spectrometry of micellar solutions, Anal. Chim. Acta 386 (1999) 287–296, https://doi.org/10.1016/S0003-2670(99)00046-X.
[57] J. Kestin, M. Sokolov, W.A. Wakeham, Viscosity of liquid water in the range −8°C to 150°C, J. Phys. Chem. Ref. Data 7 (1978) 941–948, https://doi.org/10.1063/1.555581.
[58] V. Hendrikx, J. Charvolin, M. Rawiso, L. Liebert, M.C. Holmes, Anisotropic aggregates of amphiphilic molecules in lyotropic nematic phases, J. Phys. Chem. 87 (1983) 3991–3999, https://doi.org/10.1021/j100243a039.
[59] P.R.G. Fernandes, A.A. Neto, M.A. Santos, B.F. Oliveira, H. Mukai, Light-induced birefringence in the isotropic phase of a lyotropic liquid crystal, J. Mol. Liq. 292 (2019) 111364, https://doi.org/10.1016/j.molliq.2019.111364.